IMPACT OF SURFACE AERATIONON SCALE-UP

WITH AEROBIC BIOREACTORS

by

John Birmingham

A thesis submitted to the Faculty of the University of Delaware in partial fulfillment of the requirements for the degree of Honors Degree in Chemical Engineering with Distinction

Spring 2014

IMPACT OF SURFACE AERATIONON SCALE-UP

WITH AEROBIC BIOREACTORS

by

John Birmingham

Approved: _____

Richard K. Grenville, Ph.D.
Professor in charge of thesis on behalf of the Advisory Committee

Approved: _____

Art Etchells, Ph.D.
Committee member from the Department of Chemical & Biomolecular Engineering

Approved: _____

Susan Groh, Ph.D.
Committee member from the Board of Senior Thesis Readers

Approved: _____

Michael Arnold, Ph.D.
Directory, University Honors Program

ACKNOWLEDGMENTS

I would like to thank my family and friends in particular for their love and support throughout my life and education.

I would also like to thank Dr. Grenville for taking me under his wing during my final year at University of Delaware. The elective course taught by himself and Dr. Etchells first sparked my interest in the field of mixing, and engaging in this thesis only stoked that fire. I have thoroughly enjoyed working with Dr. Grenville, and his insights were invaluable in completing this project.

I would like to thank Philadelphia Mixing Solutions, Ltd. for sponsoring my visit to their facility in Palmyra, PA. The use of their fermentation equipment made the scale-up portion of this work possible. In addition, Jason Giacomelli's help with the large scale testing was especially appreciated. My thanks also extend to Professor Dhurjati at University of Delaware, for volunteering the laboratory-scale fermentation equipment used in this work.

TABLE OF CONTENTS

LIST OF TABLES

LIST OF FIGURES

ABSTRACT

Gas-liquid mass transfer was examined on scale-up from a laboratory-scale fermentor (~1.3 L) to larger bioreactors (20-145 L). Correlations were developed to model the lumped mass transfer coefficient (k_La) as a function of gassed power input per unit volume and the superficial gas velocity. The k_La values were estimated using the Dynamic Gassing Method and the Dynamic Sulfite Method for the laboratory-scale and larger scale vessels, respectively. Air and deionized water were used as the system, and dissolved oxygen probe dynamics were incorporated. Data from the smaller bioreactor did not correlate well with the k_La values obtained at larger scales; however, the data from the two larger bioreactors were well described by a single correlation.

Surface aeration enhancement was estimated for all three bioreactors and was determined to decrease with increasing bioreactor size and increasing superficial gas velocity. The maximum enhancement due to surface aeration corresponded to less than 9% of the total measured k_La. Results compared well with literature predictions of surface aeration under sparged conditions.

Chapter 1

INTRODUCTION

1.1 Motivation

Aerobic fermentation plays a crucial role in areas as diverse as waste treatment, food processing, and the biochemical/biopharmaceutical industries[1-3]. For example, production of vinegar on a global scale only became possible with processes designed for large aerated stirred-tank fermenters[4]; such production techniques support nearly half a billion dollars in yearly worldwide vinegar exports[5]. In the biopharmaceutical market, recombinant proteins used in biologic drugs are frequently synthesized in aerobic bioreactors with prokaryotic hosts such as *Escherichia coli*[3]. Biologic drugs are currently amongst the top selling fraction of pharmaceuticals, with 2010 sales in the United States alone exceeding $30 billion dollars[6-7].

In fermentation processes such as the ones described above, carefully cultivated microorganisms consume nutrients in order to reproduce and ultimately generate a desired product. Aerobic processes in particular prove challenging as the microorganisms also require oxygen, which is only sparingly soluble in typical fermentation broths. Unless the liquid broth remains sufficiently oxygenated the cell growth rate decreases, and in the case of prolonged oxygen starvation the cells are permanently damaged or die[8]. While processes with high cell density cultures are desirable to improve product yields, meeting the cells' oxygen demand becomes a critical issue as depletion of oxygen occurs as a correspondingly faster rate[3]. To solve this problem aerobic fermentation units incorporate aeration and agitation systems, as

illustrated in Figure 1. Air is sparged in at the base of the tank and one or more impellers above the sparger break up the gas stream and keep the liquid phase well-mixed. Radial impellers are employed directly above the sparger to better shear the rising gas bubbles and reduce their size. The increase in surface area also increases the overall rate of oxygen transfer from the gas to the liquid phase. Above the first impeller, either axial flow or additional radial impellers further decrease the average gas bubble size and recirculate the liquid phase. Aerobic fermenters typically have an aspect ratio (H/T) greater than one, as taller columns increase the residence time of the gas phase and provide more surface area for heat transfer.

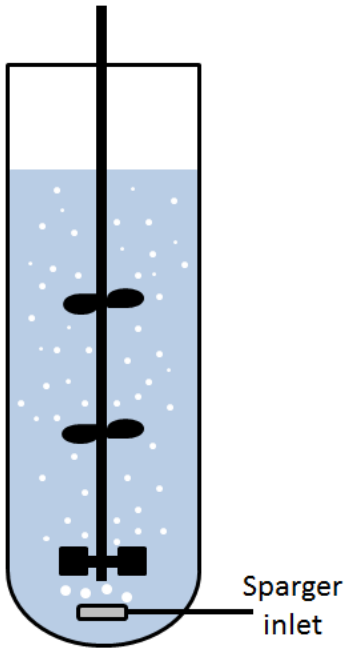

Figure 1: Illustration of a typical industrial fermenter.

One of the greatest difficulties in developing new fermentation processes lies in scaling up from small laboratory-sized units to full production on industrial equipment[1,9,10]. Successful scale up requires rigorous understanding of the oxygen transfer rate to the liquid, which is characterized by the lumped mass transfer coefficient (k_La). Specifically, the general consensus in the literature calls for scaling up aerobic fermentation processes while maintaining a constant k_La [11]. However, a complicating factor can arise due to the impact of surface aeration on mass transfer data collected at the laboratory scale[12,13]. Surface aeration occurs when air is drawn down from the headspace and entrained in the liquid phase through surface vortices; the net effect is a noticeable increase in the experimentally determined k_La values at the laboratory scale. When increasing capacity to industrial sized processes the surface area to volume ratio drops sharply, such that the effect of surface aeration becomes negligible[12,14]. By scaling up from laboratory data the k_La – and thus the total oxygen transfer rate – could be significantly overestimated. A lower k_La than predicted could lead to oxygen starvation and reduced performance of the large scale fermenter.

To improve chances of successful scale up most companies first construct a pilot plant, where further experimental testing allows the company to refine the final design for the industrial-sized process. Following this approach improves the likelihood of success of the industrial bioreactor; however, the costs in capital and lost time during the pilot plant stage are considerable. In particular, many pharmaceutical products face a narrow time window of profitability before the patent on the drug expires and generic copies can enter the market. Thus, time saved by improved scaling estimates of parameters such as k_La proves extremely valuable to the companies involved.

The main objective of the current work was the development of approximate guidelines for the impact of surface aeration of k_La and process economics when scaling up from a laboratory size fermenter. The guidelines were intended to serve as estimations for preliminary costing purposes.

Chapter 2

MEASUREMENT AND PREDICTION OF k_La

2.1 Governing Model Equations

2.1.1 Full Model Derivation

With sufficient agitation, the liquid phase can be assumed perfectly back-mixed[15]. Thus the liquid dissolved oxygen concentration (C_L) can be modeled by Equation 1, where k_La is the lumped mass transfer coefficient and C_L^* is the saturation concentration.

$$\frac{dC_L}{dt} = k_La(C_L^* - C_L) \tag{1}$$

However, conflicting options exist in the literature over whether the gas phase can be reasonably modeled as perfectly back-mixed, perfectly plug-flow, or a mixed-flow model[15-25]. In tanks with aspect ratios (H/T) much greater than unity or with viscous solutions, in particular, plug-flow models describe the system dynamics more accurately than perfectly back-mixed models[15,22,26]. For non-viscous solutions with H/T ≤ 1 many literature sources have confirmed the validity of assuming perfect back-mixing for the gas phase[15-19,21], which results in Equation (2)2 ignoring simultaneous nitrogen transport. Literature sources report less than 7% error for neglecting nitrogen transport at lower mass transfer rates[27] ($k_La \leq 0.1\ s^{-1}$).

$$V_G\frac{dC_G}{dt} = Q\left(C_{G_o} - C_G\right) - k_LaV(C_L^* - C_L) \tag{2}$$

Where the variables V, V_G, Q, C_{G_o}, and C_G are defined as follows: liquid phase volume, gas phase volume, gas volumetric flow rate, inlet gas oxygen concentration, and outlet gas oxygen concentration. The variables V_L, V_G, Q, and C_{G_o} are taken as constant with time, while C_G is assumed constant throughout the reactor for the perfectly back-mixed model.

If the absorption term in Equation 2 is assumed to be negligible, as proposed by Dang, Karrer, and Dunn[21], the gas phase response to a step change in the inlet gas concentration is given by Equation 3.

$$C_G = C_{G_o}\left(1 - \mathrm{e}^{-\frac{\mathrm{t}}{\tau_G}}\right) \tag{3}$$

Where $\tau_G = V_G/Q$ and is the gas mean residence time. Literature sources refer to a variation of this model as the "start up model", given that the initial flushing and reestablishing of the steady state gas holdup is accounted for[28]. If the gas holdup is significant, ignoring the gas holdup formation results in overestimating the driving force term in Equation 1 which leads to underestimating k_La [15,28]. Combining Equations 1 and 3 with a Henry's law constant H results in Equation 4.

$$\frac{dC_L}{dt} = k_L a\left[HC_{G_o}\left(1 - \mathrm{e}^{-\frac{\mathrm{t}}{\tau_G}}\right) - C_L\right] \tag{4}$$

A further complicating factor arises when measuring the liquid phase oxygen concentration. Convolution of the mass transfer data and the oxygen probe dynamics becomes more and more significant as k_La approaches the characteristic probe response time. For Clark-type membrane-covered polarographic oxygen electrode sensors, literature sources report use of first or second order models to capture the probe dynamics[20,21,24-26,29] . With highly viscous solutions, diffusion film effects dominate the probe response and a second order model should be employed[21].

However, with nonviscous solutions the probe response can be captured reasonably well by a first order model[20,21,25,26,29] with a time constant, τ_E. Equation 5 shows the form of a solution of the resulting set of differential equations for the measured liquid phase oxygen concentration, $C_E(t)$.

$$C_E(t) = \alpha_1 e^{-k_L a t} + \alpha_2 e^{-\frac{t}{\tau_E}} + \alpha_3 e^{-\frac{t}{\tau_G}} + \alpha_4 \quad (5)$$

2.1.2 Model Simplification

Literature sources frequently assume at least one of two limiting scenarios when analyzing k_La experimental data. Calderbank proposed setting the gas phase holdup equal to zero, as the holdup is typically small for nonviscous solutions[30]. This corresponds to $\tau_G \to 0$, which simplifies Equation 5 to the form shown in Equation 6.

$$C_E(t) = \alpha_1 e^{-k_L a t} + \alpha_2 e^{-\frac{t}{\tau_E}} + \alpha_4 \quad (6)$$

If the probe dynamics occur significantly faster than the rate of oxygen transfer, the impact of the oxygen sensor can be safely ignored[15,31,32]. Van't Riet[15] reported maximum errors in k_La of less than 6% for $\tau_E \leq 1/k_L a$, and Linek[32] determined errors due to probe response were limited to $< 3\%$ for $\tau_E \leq 1/5k_L a$. For fast-response oxygen probes, or slow mass transfer rates, neglecting the probe dynamics simplifies Equation 5 to the form shown in Equation 7.

$$C_E(t) = \alpha_1 e^{-k_L a t} + \alpha_3 e^{-\frac{t}{\tau_G}} + \alpha_4 \quad (7)$$

In the event that both the gas holdup and probe dynamics are neglected, Equation 5 can be expressed in a simple form by Equation 8.

$$C_E(t) = H C_{G_o}(1 - e^{-k_L a t}) + C_E(t = 0) \quad (8)$$

The largest gas phase holdup measured during the course of the experiments was less than 5% of the total liquid volume. As such, τ_G was taken as negligible and the simplified model proposed in Equation 6 was used to describe the system. The contribution of the dissolved oxygen probe dynamics could not be ignored, however. The dissolved oxygen probe used in the small scale experiments had a comparatively large time constant in comparison to state of the art fast-response probes, and reducing the model to Equation 8 introduced significant error into the calculations. Equation 6 was thus taken as the governing equation, and a derivation of the constants can be found in Appendix A.

2.2 Methods of Measuring k_La

Many methods exist in the literature for estimating the lumped mass transfer coefficient in sparged, agitated bioreactors. Four of the most common techniques are discussed in Sections 2.1.1-2.1.4, and both the dynamic gassing-in and the dynamic sulfite methods were implemented in the determination of experimental k_La values.

2.2.1 Dynamic Gassing-in Method (DGM)

Variants of the DGM were among the first measurement[33] techniques used to estimate k_La. The liquid phase is first stripped of oxygen through sparging nitrogen into the heavily agitated vessel. Once deoxygenated, the nitrogen gas flow is immediately switched to either air or enriched oxygen gas, and the liquid-phase oxygen concentration increases towards saturation. By monitoring $C_L(t)$ through the use of dissolved oxygen sensors, the value of k_La can be determined from a least squares regression of Equation 6, provided τ_E is known. The value of the probe time constant is determined separately, through measuring the response to a step change in the liquid phase oxygen concentration. A step change is accomplished by rapidly moving the oxygen probe from a solution deoxygenated by nitrogen stripping to an oxygen saturated solution. The change in dissolved oxygen concentration is then modeled by Equation 9, which results in Equation 10 upon integration.

$$\frac{dC_E}{dt} = \frac{HC_{G_o} - C_E(t)}{\tau_E} \tag{9}$$

$$\ln\left(HC_{G_o} - C_E(t)\right) = -\frac{1}{\tau_E}t \tag{10}$$

The value of τ_E is then estimated from the straight line slope of a plot of $\ln\left(HC_{G_o} - C_E(t)\right)$ versus time.

2.2.2 Dynamic Sulfite Method (DSM)

The DSM relies upon the instantaneous reaction of sulfite with dissolved oxygen to form sulfate, as shown in Equation 11. The 1991 American Society of Civil Engineers Standard[34] recommends addition of cobalt catalyst to reach a concentration of 0.05 mg/L (~$9 \cdot 10^{-7}$ M) of cobaltous ions. However, most literature sources[26] report a range of cobalt catalyst concentrations of 10^{-5}-10^{-6} M Co^{2+}, with some sources using up to ~10^{-3} M Co^{2+} to ensure complete and homogenous consumption of the sulfite[20].

$$SO_3^{2-} + \frac{1}{2} O_2 \xrightarrow{Co^{2+}} SO_4^{2-} \tag{11}$$

At the start of the DSM, the saturated oxygen concentration is initially reached through sparging air or enriched oxygen gas into the agitated vessel. The agitation speed and gas flow rate are maintained constant throughout the experiment, and the vessel is then charged with cobalt chloride. After allowing for the dissolution of the catalyst, the fermentor is charged with a sufficient quantity of sodium sulfite to completely consume all the dissolved oxygen in the liquid phase. The measured oxygen concentration then sharply decreases. After all of the sulfite reacts, the dissolved oxygen concentration rises toward saturation, and k_La is estimated from a least squares regression of Equation 6. Multiple experimental runs can be performed by subsequent additions of sodium sulfite charges; however, the [Na_2SO_3] is kept below 0.025 M to minimize non-coalescing behavior.

Use of DSM assumes that the sulfite reacts completely before the dissolved oxygen concentration rises, and literature sources report the assumption may fail with insufficient catalyst addition[20]. However, validation is possible by simultaneously monitoring the system pH. As the sulfite addition increases the pH, one can qualitatively assess the amount of sulfite remaining by tracking the pH profile as the

sulfite is consumed. Negligible error is incurred if the pH declines to near the pre-sulfite addition levels before the dissolved oxygen concentration increases.

2.2.3 Dynamic Pressure Method (DPM)

The DPM for measuring k_La involves a small step increase in the vessel pressure, typically executed by briefly throttling the gas outlet[33]. A pressure increase of 17-20 kPa proves sufficient and occurs in less than 0.3 seconds[27,33]. By measuring both the total pressure and the dissolved oxygen concentration, the k_La can be estimated from a set of differential material balances. The main advantage lies in the ability to change the oxygen composition in all gas bubbles simultaneously, through the increase in total system pressure[27]. As such, the assumption of a perfectly back-mixed gas phase remains valid, and many sources champion DPM as the most accurate way to measure the lumped mass transfer coefficient[26,27,33,35].

2.2.4 Steady State Sulfite Method (SSM)

Much like the DSM, the steady state sulfite method involves using the reaction shown in Equation 11 to estimate k_La. The procedure follows the DSM; however, a significantly larger excess of Na_2SO_3 is charged to the vessel. The dissolved oxygen concentration then remains essentially zero for a measured timespan usually on the order of minutes[33,36]. With accurate kinetic rate models for the reaction, the k_La can be determined knowing only the time of the reaction and the initial mass of sodium sulfite added. Yet a great deal of controversy exists in the literature as to the proper kinetics for the reaction[37-41]. In addition, many sources report substantial overestimations of k_La using the SSM[29,31,33].

2.3 Prediction of k_La from Empirical Correlations

The breadth of available literature correlations demonstrates the extensive effort to successfully model and predict the lumped mass transfer coefficient in aerated fermenters. Section 2.3.1 summarizes the general form of k_La correlations seen in the literature.

2.3.1 Correlations Dependent on Gassed Power Input

Literature sources frequently correlate k_La with power input per unit volume (P_g/V_L) and superficial gas velocity (v_{SG}) as shown in Equation 12.

$$k_La = A\left(\frac{P_g}{V_L}\right)^{\alpha}(v_{SG})^{\beta} \tag{12}$$

Where gassed power can be directly measured or predicted using the Bakker[42] relationship for Rushton turbines as shown in Equation 13.

$$P_g = P_u(1-(0.72-0.72\cdot\mu)Fr^{0.25}\tanh(24\cdot Ae)) \tag{13}$$

The variables Fr and Ae represent the Froude number and the Aeration number, respectively, and are defined in Equations 14 and 15. The ungassed power (P_u) is calculated from operating conditions, geometric parameters, and the power number (N_p) as shown in Equation 16.

$$Fr = N^2D/g \tag{14}$$

$$Ae = Q/ND^3 \tag{15}$$

$$P_u = N_p\rho N^3D^5 \tag{16}$$

Table 1 provides literature examples of correlations of the form Equation 12. As seen from the variability in predicted values of A, α, and β no single correlation accurately predicts k_La over all systems of interest.

Table 1: k_La correlations for coalescing systems based on power input.

Author	Year Published	Correlation	T (in.)	D/T	System	Measurement Method
Smith et. al.[45]	1977	$k_La = 0.01\left(\frac{P_g}{V}\right)^{0.475} v_{SG}^{0.4}$	24 - 72	0.33 – 0.5	Air – Water	---
Van't Riet[15]	1979	$k_La = 0.026\left(\frac{P_g}{V}\right)^{0.4} v_{SG}^{0.5}$	---	---	Air - Water	DGM
Chandrasekharan and Calderbank[24]	1980	$k_La = 0.0287 \cdot T^{2.01T^{-0.59}-3.911}\left(\frac{P_g}{V}\right)^{0.563} v_{SG}^{0.631}$	48	0.297	O_2 - Water	DGM variant
Moresi and Patete[22]	1988	$k_La = 0.0229\left(\frac{P_g}{V}\right)^{0.756}\left(\frac{Q}{V_L}\right)^{0.81}$	8.98 – 102.4	0.214 – 0.455	Air - Na_2SO_4 Soln.	SSM
Linek et. al.[27]	1992	$k_La = 0.00384\left(\frac{P_g}{V}\right)^{0.654} v_{SG}^{0.4}$	11.42	1/3	Air – Water	DPM
Wu[46]	1995	$k_La = 1.06\left(\frac{P_g}{V}\right)^{0.67} v_{SG}^{0.56}$	7.95 and 12	1/2	Air – Water	SSM
Vilaça et. al.[36]	2000	$k_La = 0.00676\left(\frac{P_g}{V}\right)^{0.94} v_{SG}^{0.65}$	8.27	0.405	Air – Water	SSM
Linek et. al.[47]	2004	$k_La = 0.0108\left(\frac{P_g}{V}\right)^{0.699} v_{SG}^{0.581}$	11.42	1/3	O_2 – Water	DPM
Puskeiler and Weuster-Botz[20]	2005	$k_La = 0.00135\left(\frac{P_g}{V}\right)^{1.278} v_{SG}^{0.4}$	---	---	O_2 – Na_2SO_4 Soln.	SSM variant
Fujasová, Linek, and Moucha[35]	2006	$k_La = 0.00487\left(\frac{P_g}{V}\right)^{0.719} v_{SG}^{0.497}$	11.42	1/3	Air – Water	DPM
Gill et. al.[48]	2008	$k_La = 0.224\left(\frac{P_g}{V}\right)^{0.35} v_{SG}^{0.52}$	2.36	1/3	Fermentation Broth	----
Scargiali et. al.[29]	2010	$k_La = 0.0037\left(\frac{P_g}{V}\right)^{0.585} v_{SG}^{0.350}$	7.48	0.342	Air – Water	DPM variant
Karimi et. al.[1]	2013	$k_La = 0.28\left(\frac{P_g}{V}\right)^{0.67} v_{SG}^{0.58}$	3.94	1/2	Air – Water	DGM

Chapter 3

EXPERIMENTAL k_La DETERMINATION

3.1 Small Scale k_La Determination

The laboratory-scale bioreactor used in this work is shown in Figure 2, and Table 2 contains the dimensions and geometric factors of the system. The bioreactor synced with a New Brunswick BioFlo/CelliGen 115 unit used to control sparger gas flow rates and agitation speed. Deionized water was used for the experiments, and a heating jacket maintained a constant liquid temperature of 37°C. Three removable stainless steel baffles were constructed and anchored to the vessel supports to prevent vortex formation. Dissolved oxygen levels were monitored with a Mettler Toledo InPro 6800 series polarographic sensor, with a manufacturer[43] listed maximum error of ± 6 ppb. The probe dynamics were modeled as first order, and the time constant was determined as discussed in Section 2.2.1 to be 21.1 ± 0.3 seconds. Detailed calculations are included in Appendix B.

A range of agitation and gas flow rates were tested, and the results were correlated in the form described by Equation 12. Impeller speeds $300 \leq N \leq 425\ RPM$ and gas flow rates $0 \leq Q \leq 4.8\ LPM$ were tested; the gassed power in each case was calculated with the Equations 13 and 16.

Table 2: Geometric properties of laboratory-scale bioreactor.

V	T	H/T	D/T	D_s/T	h/T	b/T	w_b/T
1.3 L	4.92 in.	1	0.424	0.32	0.364	0.1	0.1

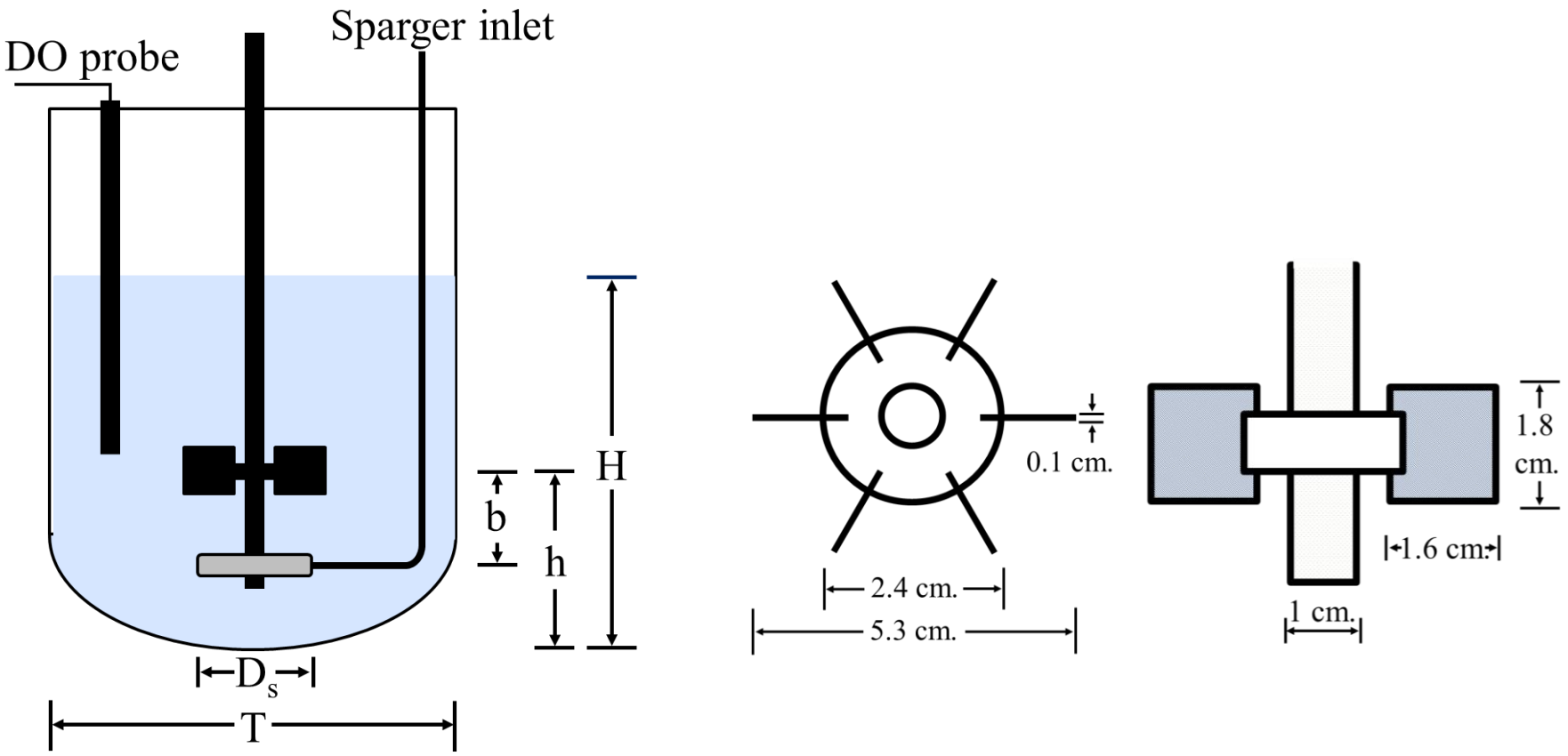

Figure 2: Schematic of laboratory-scale bioreactor.

3.1.1 Dynamic Gassing Method

The DGM was employed following the general procedure described in Section 2.2.1, with air as the gas phase (assumed ~ 20.95 mol% O_2). Figure 3 shows a sample dissolved oxygen profile, as well as the predicted profiles based on Equations 6 and 8. Although the initial dynamics of the system are not completely captured by the Equation 6, the overall fit to the data appeared sufficient. Error could have been introduced by neglecting the gas holdup, which reached a maximum at 5% of the liquid volume at high sparging and agitation rates.

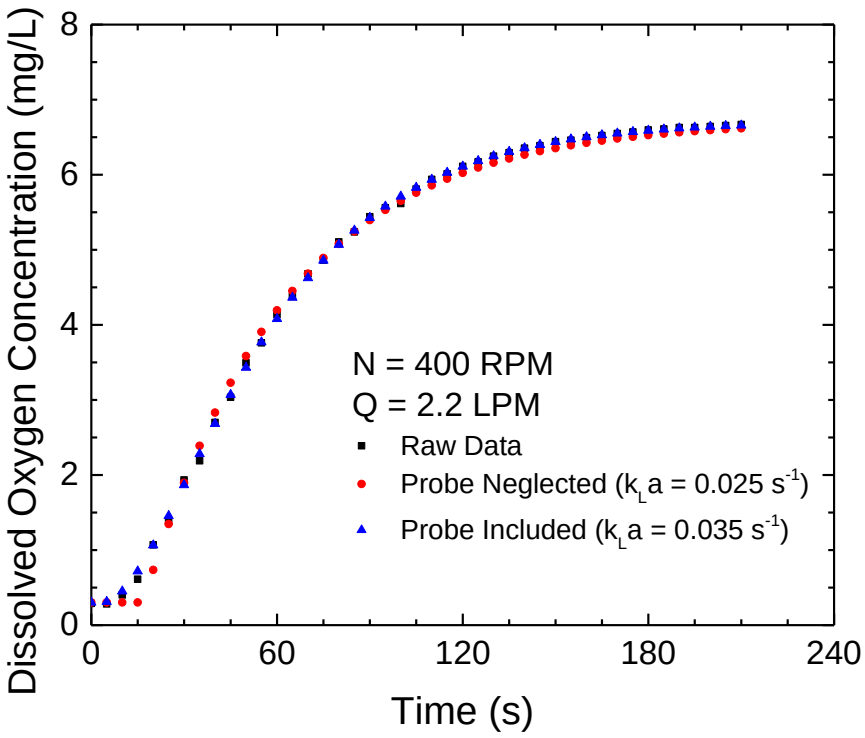

Figure 3: Dissolved oxygen profile for DGM in laboratory-scale bioreactor.

Parameters for the k_La correlation shown in Equation 12 were calculated from a multivariable regression of the data and Equation 17 shows the best-fit correlation. Figure 4 shows the collected data plotted against the obtained correlation.

$$k_L a = 0.15 \left(\frac{P_g}{V}\right)^{0.54} \nu_{SG}^{0.80} \tag{17}$$

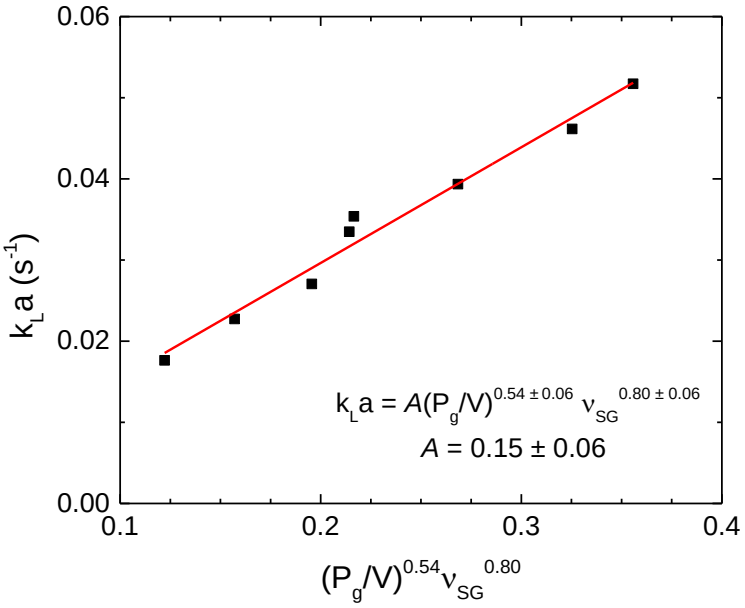

Figure 4: Lumped mass transfer coefficient correlation for laboratory-scale bioreactor.

Equation 17 fell within the expected range of literature correlations; however, the larger exponent on the superficial gas velocity showed the stronger dependence on gas flow rate at small bioreactor scales.

3.2 Determination of k_La in Larger Vessels

Scale-up data were collected using tanks with nominal diameters of 1 ft. (Tank 1) and 2 ft. (Tank 2) provided by Philadelphia Mixing Solutions, Ltd[44]. The dimensions and geometric factors for the vessels are shown in Table 3 and Figure 5. Deionized water and pressurized air were used for the experiments. The temperature ranged from 11.5-25°C; however, during each measurement the temperature change was small. Both tanks had 4 removable baffles, with dimensions given in Table 3. Tank 1 was flat bottomed, while Tank 2 had a standard ASME flanged and dished head. The dissolved oxygen levels were measured using a YSI – Pro ODO polarographic oxygen sensor, which was determined to have a time constant of ~ 5.5 seconds.

Section 2.2.2 describes the general procedure followed for the DSM in the larger bioreactor. Technical grade cobalt chloride hexahydrate from Bowman, Mell & Company, Inc. was used to catalyze the sulfite reaction, and the concentration of cobalt ions was maintained at $3.5 \cdot 10^{-6}$ M. Industrial grade sodium sulfite anhydrous from Fisher-Scientific Company was used for all experiments. Multiple experimental runs were consecutively performed; however, the fermentor system was emptied, rinsed, and refilled with deionized water when the total sodium sulfate concentration reached 0.025 M.

The best-fit parameters for Equation 12 were determined as described in Section 3.1.1, and Figure 6 shows the collected data plotted against the obtained correlation for each tank. Both correlations compare favorably with the literature examples in Table 1.

Table 3: Geometric properties of larger experimental bioreactors.

	V	T	H/T	D/T	d_W/D	d_B/D	h/T	b/T	w_b/T
Tank 1	0.71 ft^3	11.44 in.	1	0.415	0.58	0.0.13	0.364	0.1	0.09
Tank 2	5.14 ft^3	24 in.	1	0.400	0.59	0.013	0.364	0.1	0.08

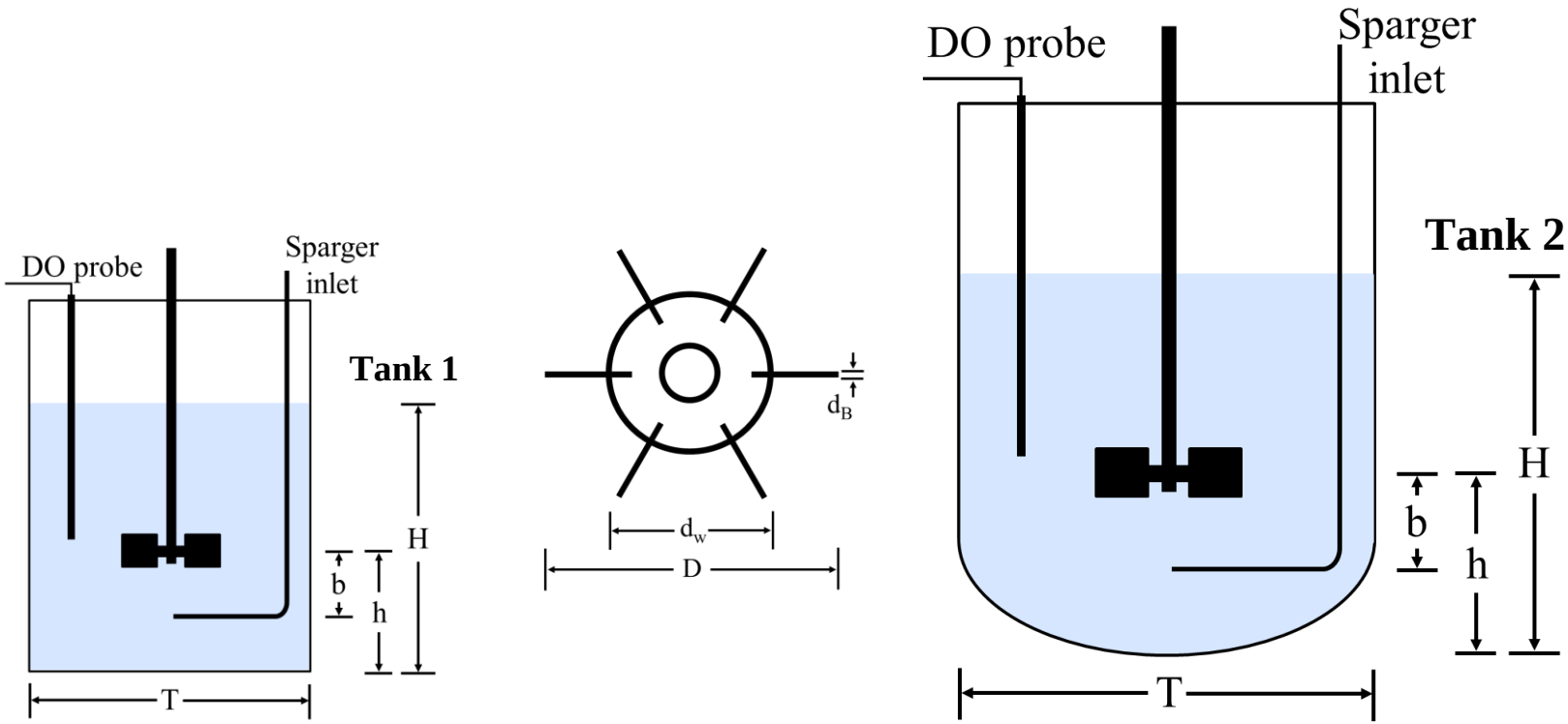

Figure 5: Schematic of larger experimental bioreactors.

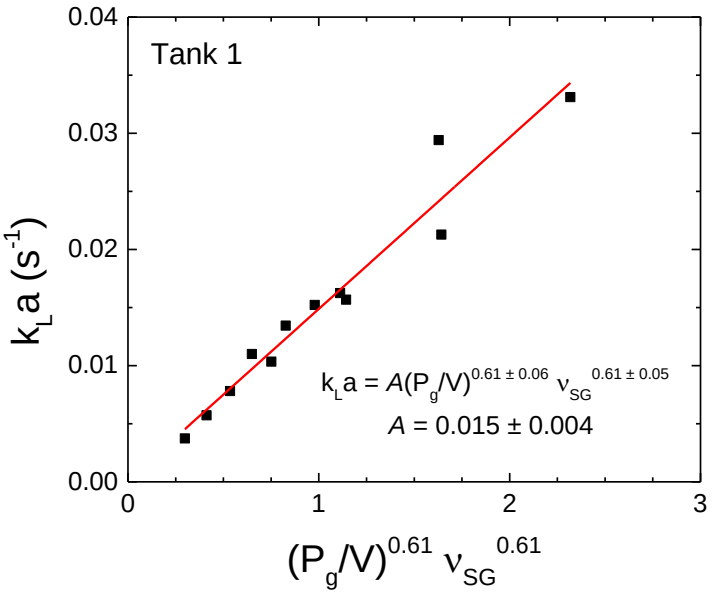

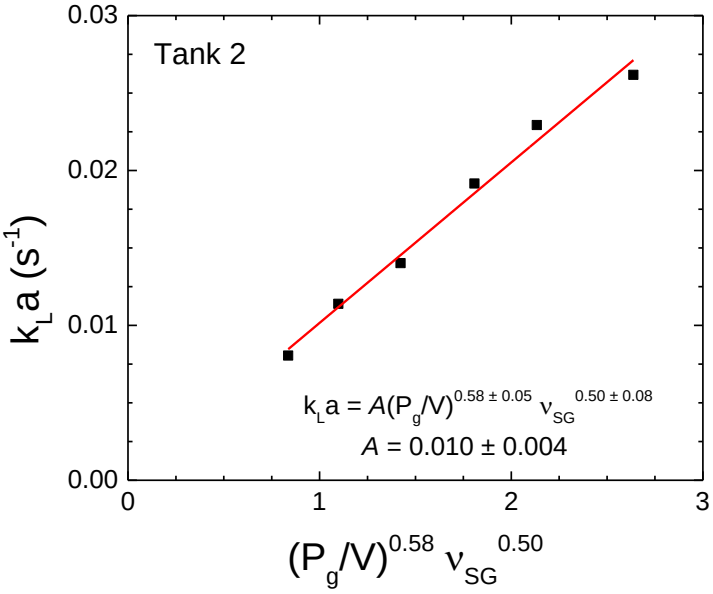

Figure 6: Lumped mass transfer coefficient correlations for Tank 1 and Tank 2.

3.3 Estimation of Scale-up for k_La and Comparison to Literature

The data obtained in all vessels was then force-fit to a combined correlation of the form of Equation 12, as shown in Figure 7. The larger tank data correlated well, while the smaller tank data showed substantial discrepancies. Possible explanations include the following:

- Neglect of gas holdup contribution
- Different measurement method – DGM vs. DSM
- Insufficient catalyst concentration for DSM
- Impact of surface aeration

In particular, the influence of surface aeration has been shown to considerably increase the measured mass transfer coefficient on small laboratory scales[12,49]. Such enhancement in mass transfer could explain the significantly higher k_La values observed (and therefore the larger value of the parameter A in Equation 17) in the laboratory-scale bioreactor.

It has been shown that the surface aeration rate decreases rapidly with increasing gas flow rate[51]. The physical justification for this stems from the decrease in liquid pumping capability of the agitator at higher gas loading, which results in fewer gas-entraining surface vortices. In addition, sources report that increasing gas flow rates "physically repels downflow" of gas in the headspace[51]. The potential impact of surface aeration on the mass transfer rate is further examined in Chapter 4.

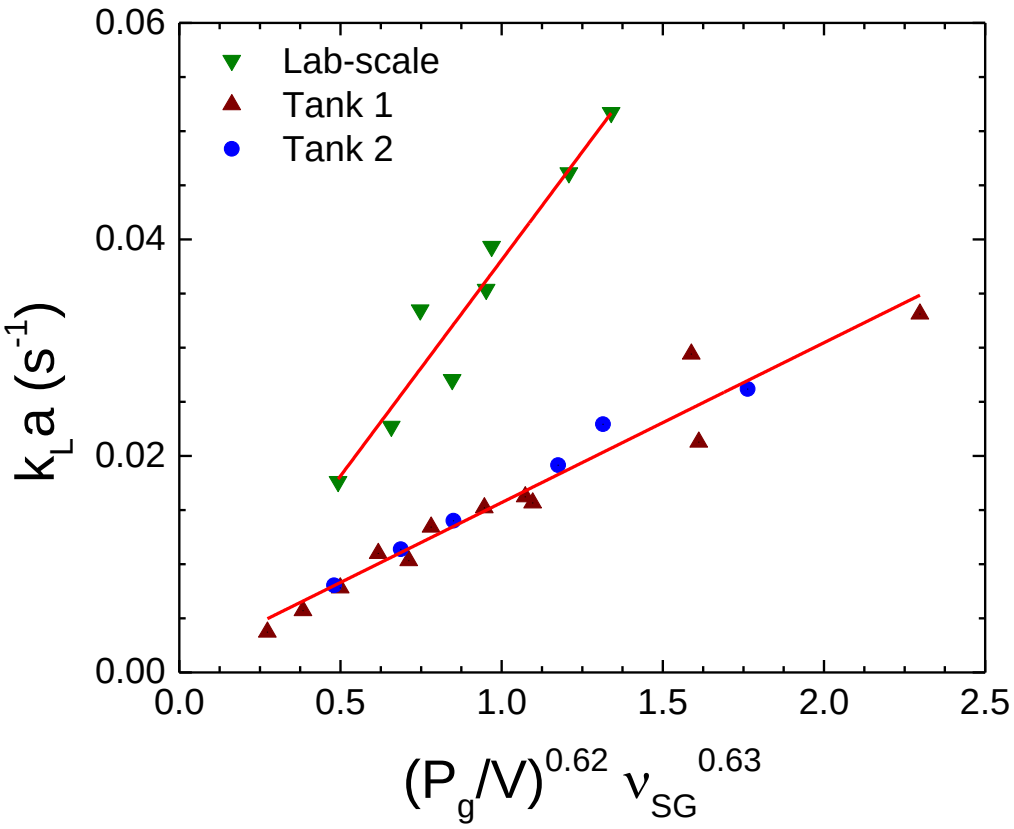

Figure 7: Combined lumped mass transfer data for all vessels.

The data from the two larger bioreactors correlates well, which supports the literature recommendation of avoiding scale-up based on vessels under 200 L in volume[12]. Equation 18 shows the correlation determined for the combined Tank 1 and Tank 2 data.

$$k_L a = 0.014 \left(\frac{P_g}{V}\right)^{0.63} \nu_{SG}^{0.63} \tag{18}$$

Chapter 4

IMPACT OF SURFACE AERATION ON k_La AND SCALE-UP

The impact of surface aeration on mass transfer measurements has been discussed in Section 3.3. Enhancements in the observed k_La at small scales do not transfer to larger scales due to the decrease in the surface area to volume ratio. In particular, pilot plant and industrial bioreactors often operate with aspect ratios between one and three, which further reduces the area over which surface aeration could occur. If scale-up predictions based on laboratory-scale data do not consider surface aeration, the observed k_La on scale-up may decrease substantially[12]. Further efforts were made in Sections 4.1 and 4.1 to determine the influence of surface aeration on the mass transfer data shown in Chapter 3.

4.1 Determination of Surface Aeration Effect

Baffles were removed from the laboratory-scale bioreactor described in Table 2 and Figure 2 to promote the formation of a large surface vortex near the impeller shaft. As vortices improve gas entrainment from the headspace[50], this was taken as the limiting case in which surface aeration would most contribute to the measured k_La. Measurements were taken following the DGM procedure outlined in Section 3.1 for impeller speeds $300 \leq N \leq 600\ RPM$ and gas flow rates $0 \leq Q \leq 4\ LPM$. The measurements were performed under two settings, where 2 LPM of either air or nitrogen gas was continuously flushed through the headspace to promote or suppress the influence of surface aeration, respectively.

The data for sparger flow rates of 1 LPM are shown in Figure 8, where for $Q = 0$ the mass transfer observed was strictly due surface aeration from headspace air entrainment. As expected, flushing the headspace with nitrogen gas significantly reduced the observed k_La by suppression of surface aeration. Indeed, the k_La predicted from surface aeration alone ($Q = 0$) appeared to correlate well with the observed reduction in k_La during nitrogen sparging for impeller speeds below 500 RPM. At higher agitation speeds, the observed surface vortex reached the impeller. As a result, the system reacted much the same as under sparging conditions and the observed k_La was significantly higher seen for surface aeration only at lower speeds.

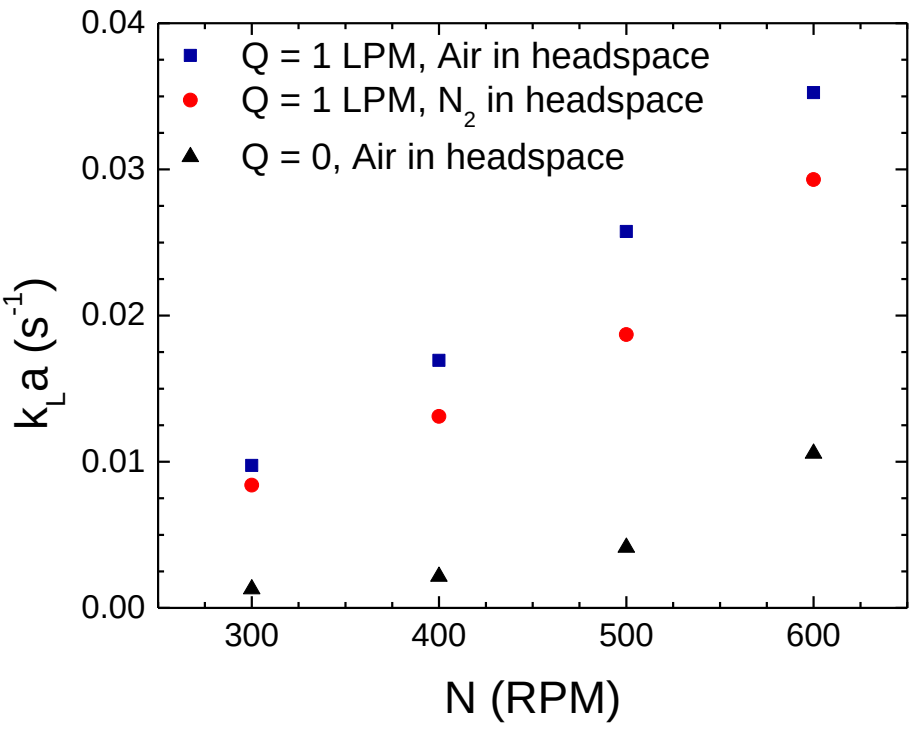

Figure 8: Surface aeration impact on unbaffled laboratory-scale bioreactor.

4.2 Surface Aeration on Scale-up

Measurements as described in Section 4.1 were performed for the baffled laboratory-scale bioreactor under unsparged conditions. Air was flushed through the headspace as discussed in Section 4.1 to ensure the gas composition at the surface remained constant. Additional DSM experiments were performed under unsparged conditions for both Tank 1 and Tank 2 as well.

Surface aeration intensity was considered as the ratio of the k_La obtained under unsparged conditions to that observed under standard sparging rates. While some literature sources report similar methodologies[12], other sources report that such a comparison overestimates the impact of surface aeration[13]. The results were thus viewed as an upper limit of the possible influence of surface aeration on process scale-up.

Figure 9 shows the ratio of $k_La_{unsparged}$ to $k_La_{sparged}$ for all three vessels. The abscissa of the plots was taken as the Froude number, which was defined in Equation 14. The Froude number represents a ratio of a system's characteristic velocity to the resultant wave propagation velocity, and as such has been used in surface aeration studies as a measure of surface agitation[51].

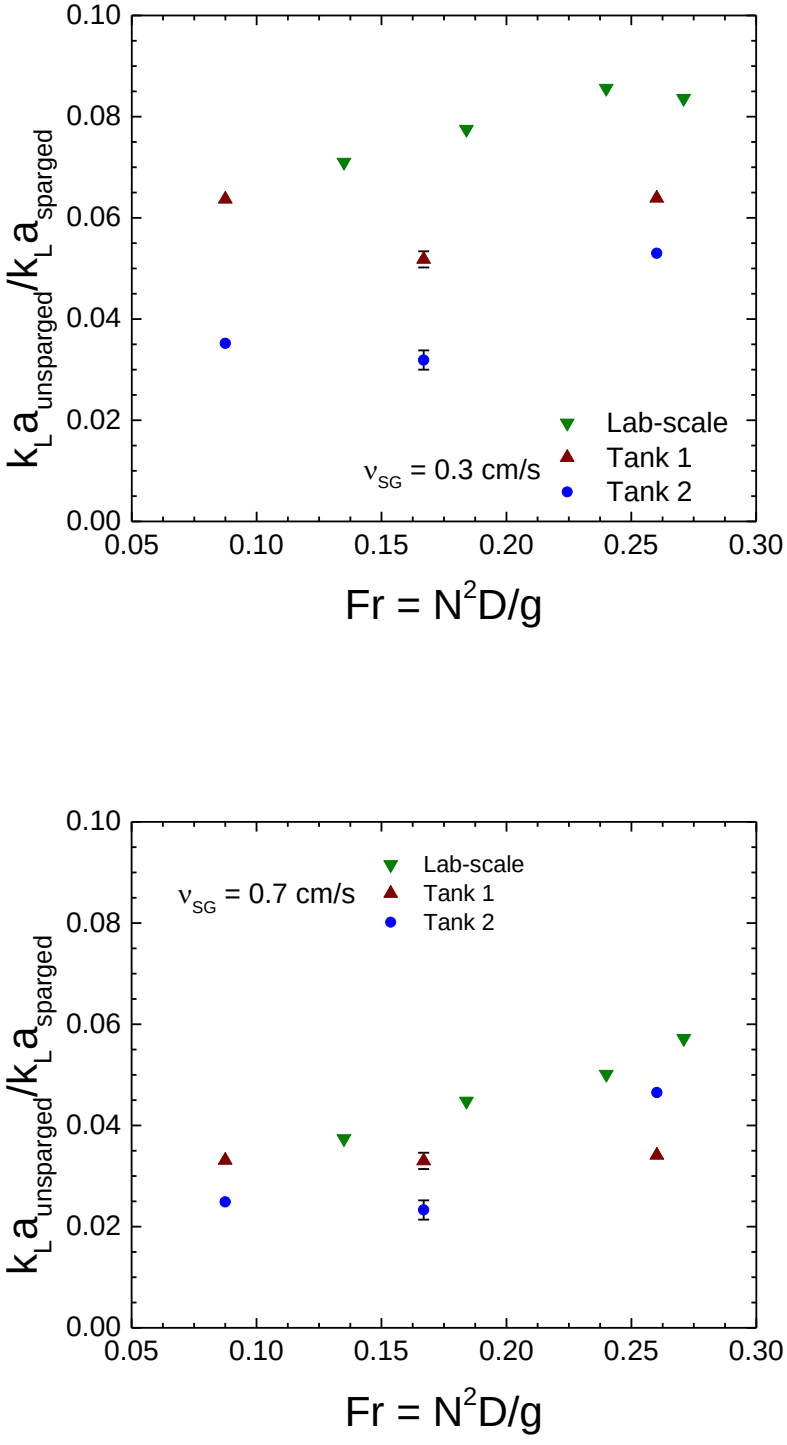

Figure 9: Ratio of $k_L a$ values under unsparged and sparged conditions.

As expected the influence of surface aeration appeared significantly more important for the smaller bioreactor than for either Tank 1 or Tank 2. The maximum observed difference in the ratio of unsparged to sparged k_La values occurred at a superficial gas velocity of 0.3 cm/s and Fr ~ 0.17. At this point the laboratory-scale bioreactor ratio was 150% larger than that of Tank 1 and nearly 250% larger than that of Tank 2. In addition, the observed influence of surface aeration decreased in all vessels with the increase in superficial gas velocity to 0.7 cm/s, as predicted in the literature[51].

The largest value of $k_La_{unsparged}/k_La_{sparged}$ measured was 0.09, corresponding to a maximum contribution of surface aeration of nearly 9% to the total measured k_La. If surface aeration proved completely negligible at an industrial scale the maximum decrease in k_La due to decreasing surface aeration enhancement would be approximately 9%. This assumes the laboratory-scale bioreactor would be scaled up to a geometrically similar industrial fermentor. In practice, an increase in both H/T and superficial gas velocity is typical on scaling up; both of these factors would further negate the influence of surface aeration in the scaled-up bioreactor, as discussed previously.

The results compare well to literature predictions of scale-up of surface aeration. Chapman, Nienow, and Middleton[13] determined under sparged conditions the rate of surface aeration never exceeded 20% - and was frequently less than 5% - of the total mass transfer rate in a 8.7 in. diameter vessel.

Chapter 5

CONCLUSIONS AND FUTURE WORK

5.1 Conclusions

The measured lumped mass transfer coefficients were well described by Equation 12 for each individual vessel size. However, the data collected at the smallest bioreactor tested did not correlate well with the k_La values measured for Tank 1 and Tank 2. Surface aeration was considered as a potential source of the discrepancy and was found to contribute in a small role. The maximum observed enhancement of k_La by surface aeration was approximately 9% of the total lumped mass transfer coefficient; however, the enhancement was generally small. Surface aeration was determined to decrease with both increasing vessel size and superficial gas velocity.

5.2 Future Work

Further examination of the conditions used for the DSM should be pursued. Literature sources have indicated that the cobalt catalyst concentration recommended by the ASCE may be insufficient, which would result in lower observed k_La values[20]. In addition, testing on the smaller laboratory-scale bioreactor should be revisited using the DSM, in order to determine how the results of the two methods compare on the same system.

REFERENCES

1. Karimi, A.; Golbabaei, F.; Mehrniam M.R.; Neghab, M.; Mohammad, K.; Nikpey, A.; Pourmand, M.R. Oxygen Mass Transfer in a Stirred Tank Bioreactor Using Different Impeller Configurations for Environmental Purposes. *Iranian J. of Envir. Health Science & Eng.* **2013**, 10.

2. Moucha, T.; Rejl, F.J.; Kordac, M.; Labik, L. Mass Transfer Characteristics of Multiple-Impeller Fermentors for their Design and Scale-up. *Biochemical Eng. Journal*. **2012**m 69, pp. 17-27.

3. Choi, J.H.; Keum, K.C.; Sang, Y.L. Production of Recombinant Proteins by High Cell Density Culture of Escherichia Coli. *Chem. Eng. Science*. **2006**, 61, pp. 876-885.

4. Tan, S.C. Vinegar Fermentation. M.S. Thesis, Louisiana State University, Baton Rouge, LA. 2005.

5. Agriculture and Agri-Food Canada. *The Global Vinegar Market: Opportunities for Canadian Vinegar Exporters*. Canada. 2011.

6. Champion, S.; Guha, R.; Salgado, M. Emerging Competition Issues in Biologics. *Antitrust Health Care Chronicle*. **2013**. 26.

7. Evans, Ian. Follow-on Biologics: A New Play for Big Pharma. *Yale Journal of Biology and Medicine*. **2010**, 83, pp. 97-100.

8. Enfors, S.O.; Jahic, M.; Rozkov, A.; Xu, B.; Hecker, M.; Jurgen, B.; Kruger, E.; et. al. Physiological Responses to Mixing in Large Scale Bioreactors. *J. of Biotechnol.* **2001**, 85, pp. 175-185.

9. Rouf, S.A.; Moo-Young, M.; Scharer, J.M.; Douglas, P.L. Single versus multiple bioreactor scale-up: economy for high-value products. *Biochemical Engineering Journal*. **2000**, 6 pp. 25-31.

10. Schmidt, F.R. Optimization and Scale Up of Industrial Fermentation Processes. *Appl. Microbiol. Biotechnol.* **2005**, 68, pp. 425-435.

11. González-Sáiz, J.; Garrido-Vidal, D.; Pizarro, C. Scale Up and Design of Processes in Aerated-stirred Fermenters for the Industrial Production of Vinegar. *J. of Food Eng.* **2009**, 93, pp. 89-100.

12. Fuchs, R.; Ryu, D.; Humphrey, A.E. Effect of Surface Aeration on Scale-Up Procedures for Fermentation Processes. *Ind. Eng. Chem. Process Des. Develop.* **1971**, 10, pp. 190-195.

13. Chapman, C.M.; Nienow, A.W.; Middleton, J.C. Surface Aeration in a Small, Agitated, and Sparged Vessel. *Biotechnol. and Bioeng.* **1980**, 12, pp. 981-993.

14. Veljković, V.; Skala, D. Effect of Number of Turbine Impellers on Surface Aeration in Laboratory Fermentor. *Biotechnol. and Bioeng.* **1989**, 34, pp. 207-213.

15. Van't Riet, K. Review of Measuring Methods and Results in Nonviscous Gas-Liquid Mass Transfer in Stirred Vessels. *Ind. Eng. Chem. Process Des. Dev.* **1979**, 18, pp. 357-364.

16. Bandyopadhyay, B.; Humphrey, A.E. Dynamic Measurement of the Volumetric Oxygen Transfer Coefficient in Fermentation Systems. *Biotech. Bioeng.* **1967**, 9, pp. 533-544.

17. Hanhart, J.; Kramers, H.; Westerterp, K.R. The Residence Time Distribution of the Gas in an Agitated Gas-Liquid Contactor. *Chem. Eng. Science.* **1963**, 18, 503-509.

18. Schlüter, V.; Deckwer, W.D. Gas/Liquid Mass Transfer in Stirred Vessels. *Chem. Eng. Science*. **1992**, 47, pp. 2357-2362.

19. Figueiredo, M.M.L.; Calderbank, P.H. The Scale-up of Aerated Mixing Vessels for Specified Oxygen Dissolution Rates. *Chem. Eng. Science*. **1979**, 34, pp. 1333-1338.

20. Puskeiler, R.; Weuster-Botz, D. Combined Sulfite Method for the Measurement of the Oxygen Transfer Coefficient k_La in Bioreactors. *J. Biotechnol.* **2005**, pp. 430-438.

21. Dang, N.D.P.; Karrer, D.A.; Dunn, I.J. Oxygen Transfer Coefficients by Dynamic Model Moment Analysis. *Biotech. Bioeng.* **1977**, 19, pp. 853-865.

22. Moresi, M.; Patete, M. Prediction of k_La in Conventional Stirred Fermenters. *J. Chem. Tech. Biotechnol.* **1988**, 42, pp. 197-210.

23. Dunn, I.J.; Einsele, A. Oxygen Transfer Coefficients by the Dynamic Method. *J. Appl. Chem. Biotechnol.* **1975**, 25, pp. 707-720.

24. Chandrasekharan, K.; Calderbank, P.H. Further Observations on the Scale-Up of Aerated Mixing Vessels. *Chem. Eng. Science.* **1981**, 36, pp. 819-823.

25. Havelka, P.; Moucha, T.; Sinkule, J.; Linek, V. Chemical Dynamic Method for Measuring k_La in Gas-Liquid Dispersions. *Chem. Eng. Comm.* **1988**, 168, pp. 97-110.

26. Pinelli, D.; Liu, Z.; Magelli, F. Analyis of k_La Measurement Methods in Stirred Vessels: The Role of Experimental Techniques and Fluid Dynamic Models. *Int. J. of Chem. Reactor Eng.* **2010**, 8.

27. Linek, V.; Benes, P.; Sinkule, J.; Moucha, T. Non-Ideal Pressure Step Method for k_La Measurement. *Chem. Eng. Science*. **1993**, 9, pp. 1593-1599.

28. Linek, V.; Benes, P.; Hovorka, F. The Role of Interphase Nitrogen Transport in the Dynamic Measurement of the Overall Volumetric Mass Transfer Coefficient in Air-Sparged Systems. *Biotechnol. and Bioeng.* **1981**, 13, pp. 301-319.

29. Scargiali, F.; Busciglio, A.; Grisafi, F.; Brucato, A. Simplified Dynaminc Pressure Method for k_La Measurement in Aerated Bioreactors. *Biochemical Eng. J.* **2010**, 49, pp. 165-172.

30. Calderbank, P.H. Physical Rate Processes in Industrial Fermentation.. *Trans. Inst. Chem. Eng.* **1959**, 37, pp. 173-185.

31. Stoker, E. Comparative Studies on Scale-Up Methods of Single-Use Bioreactors. M.S. Thesis, Utah State University, Logan, UT. 2011.

32. Linek, V. Determination of Aeration Capacity of Mechanically Agitated Vessels by a Fast Response Oxygen Probe. *Biotechnol. and Bioeng.* **1971**, 14, pp 285-289.

33. Gogate, P.R.; Pandit, A.B. Survey of Measurement Techniques for Gas-Liquid Mass Transfer Coefficient in Bioreactors. *Biochem. Eng. J.* **1999**, 4, pp. 7-15.

34. Stenstrom, M.K.; Leu, S.; Jiang, P. Theory to Practice: Oxygen Transfer and the New ASCE Standard. *WEFTEC*. **2006**.

35. Fukasová, M.; Linek, V.; Moucha, T. Mass Transfer Correlations for Mutliple-Impeller Gas-Liquid Contactors. *Chem. Eng. Science*. **2007**, 62, pp. 1650-1669.

36. Vilaca, P.R.; Badino, A.C.; Facciotti, M.R.; Schmidell, W. Determination of Power Consumption and Volumetric Oxygen Transfer Coefficient in Bioreactors. *Bioprocess Eng.* **2000**, 22, pp. 261-265.

37. Linek, V.; Vacek, V. Chemical Engineering Use of Catalyzed Sulfite Oxidation Kinetics for the Determination of Mass Transfer Characteristics of Gas-Liquid Contactors. *Chem. Eng. Science*. **1981**, 11, pp. 1747-1768.

38. Bengtsson, S.; Bjerle, I. Catalytic Oxidation of Sulphite in Diluted Aqueous Solutions. *Chem. Eng. Science*. **1975**, 30, pp. 1429-1435.

39. De Waal, K.J.A.; Okeson, J.C. The Oxidation of Aqueous Sodium Sulphite Solutions. *Chem. Eng. Science*. **1966**, 21, pp. 559-572.

40. Shaikh, A.A.; Zaidi, S.M.J. Kinetics of Catalytic Oxidation of Aqueous Sodium Sulfite. *React. Kinet. Catal. Lett.* **1998**, 64, pp. 343-349.

41. Sivaji, K.; Murty, G.S.R.N. Kinetics of Sulfite Oxidation Reaction. *Ind. Eng. Chem. Fundam.* **1982**, 21, pp. 344-352.

42. Bakker, A.; Myers, K.J.; Smith, J.M. How to Disperse Gases in Liquids. *Chem. Eng.* **1994**, 101.12, pp. 98-104.

43. Mettler Toledo, *InPro 6800 Polarographic Oxygen Sensor*, http://us.mt.com/us/en/home/products/Process-Analytics/DO-CO2-ozone-sensor/dissolved-oxygen-meter/InPro-6800.html?smartRedirectEvent=true, May 2014.

44. Philadelphia Mixing Solutions, Ltd. http://www.philamixers.com/.

45. Smith, J.M.; Van't Riet, K.; Middleton, J.C. Scale-Up of Agitated Gas-Liquid Reactors for Mass Transfer. Proceedings of 2nd European Conference on Mixing. **1977**. Cambridge, UK.

46. Wu, H. An Issue on Application of a Disk Turbine for Gas-Liquid Mass Transfer. *Chem. Eng. Science*. **1995**, 17, pp. 2801-2811.

47. Linek, V.; Kordac, M.; Fujasová, M.; Moucha, T. Gas-Liquid Mass Transfer Coefficient in Stirred Tanks Interpreted Through Models of Idealized Eddy Structure of Turbulence in the Bubble Vicinity. *Chem. Eng. And Processing*. **2004**, 43, pp. 1511-1517.

48. Gill, N.K.; Appleton, M.; Baganz, F.; Lye, G.J. Quantification of Power Consumption and Oxygen Transfer Characteristics of a Stirred Miniature Bioreactor for Predictive Fermentation Scale-Up. *Biotechnol. and Bioeng.* **2008**, 100.

49. Junker, B.H. Scale-Up Methodologies for *Escherichia coli* and Yeast Fermentation Processes. *J. Bioscience and Bioengineering*. **2004**, 97, pp. 347-364.

50. Grenville, R.K.; Etchells, A.W. Gas-Liquid Mixing. Presented at University of Delaware, Newark, DE, 2013.

51. Rao, A.; Bimlesh, K. Scale Up Parameter for Surface Aeration Systems. *Int. J. Chem. Reactor Eng.* **2008**, 6.

Appendix A

MODEL EQUATION DERIVATION

The model shown in Equation 6 was derived using the method of Laplace transforms and the process flow diagram shown in Figure 10.

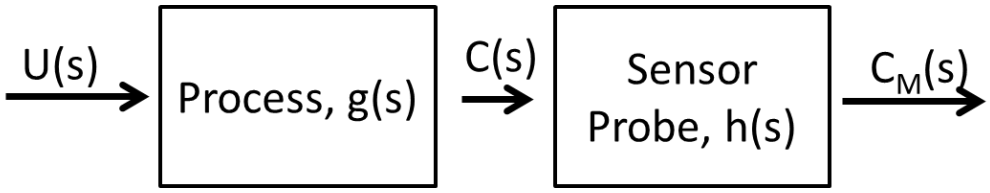

Figure 10: Process flow diagram for model derivation.

With deviation variables $U(t)$, $C(t)$, and $C_E(t)$ defined in Equations 18-20 and $C_E(t)$ is the measured dissolved oxygen concentration.

$$U(t) = C_L^*(t) - C_L^*(t=0) \tag{19}$$

$$C(t) = C_L(t) - C_L(t=0) = C_L(t) - C_L^*(t=0) \tag{20}$$

$$C_M(t) = C_E(t) - C_E(t=0) = C_M(t) - C_L^*(t=0) \tag{21}$$

The derivation considered the process as involving a step change in the saturation concentration of oxygen in the liquid phase, either as the nitrogen sparge was switched to oxygen (DGM) or as the sulfite was completely consumed (DSM). Before $t = 0$, the whole system was taken to be at equilibrium.

Starting with Equation 1, and assuming first order dynamics for the dissolved oxygen probe with a time delay of β, the transfer functions $g(s)$ and $h(s)$ were defined by Equations 21 and 22.

$$g(s) = \frac{1}{\tau_p s + 1}; \qquad \tau_p = \frac{1}{k_L a} \tag{22}$$

$$h(s) = \frac{1}{\tau_E s + 1} e^{-\beta s} \tag{23}$$

The measured concentration as shown in Equation 6 was simplified with partial fractions and inverted to yield Equation 27.

$$C_M(s) = \frac{HC_{G_o} - C_E(t=0)}{s} \cdot g(s) \cdot h(s) \tag{24}$$

$$C_M(t) = \left(HC_{G_o} - C_E(t=0)\right) \cdot \left[\left(\frac{1}{\frac{\tau_p}{\tau_E} - 1}\right) e^{-\frac{(t-\beta)}{\tau_E}} + \left(\frac{1}{\frac{\tau_E}{\tau_P} - 1}\right) e^{-\frac{(t-\beta)}{\tau_p}} + 1\right] \tag{25}$$

$$C_E(t) = C_E(t=0) + \left(HC_{G_o} - C_E(t=0)\right) \cdot \left[\left(\frac{1}{\frac{\tau_p}{\tau_E} - 1}\right) e^{-\frac{(t-\beta)}{\tau_E}} + \left(\frac{1}{\frac{\tau_E}{\tau_P} - 1}\right) e^{-\frac{(t-\beta)}{\tau_p}} + 1\right] \tag{26}$$

The corresponds to Equation 6 with the change of variables $t = t - \beta$ and the variables α_1, α_2, and α_4 defined in Equations 26 through 28.

$$\alpha_1 = \left(HC_{G_o} - C_E(t=0)\right) \cdot \left(\frac{1}{\frac{\tau_E}{\tau_P} - 1}\right) \tag{27}$$

$$\alpha_2 = \left(HC_{G_o} - C_E(t=0)\right) \cdot \left(\frac{1}{\frac{\tau_p}{\tau_E} - 1}\right) \tag{28}$$

$$\alpha_4 = HC_{G_o} \tag{29}$$

Appendix B

DISSOLVED OXYGEN PROBE TIME CONSTANT DETERMINATION

Both dissolved oxygen probes were considered to have first order dynamics, as discussed in Section 2.1.1. By inducing a step change in liquid phase dissolved oxygen concentration, the time constant for each probe was determined by plotting Equation 10. Figure 11 shows a sample plot of the dissolved oxygen profile as well as Equation 10 for the InPro 6800 series dissolved oxygen probe used in the laboratory-scale bioreactor system.

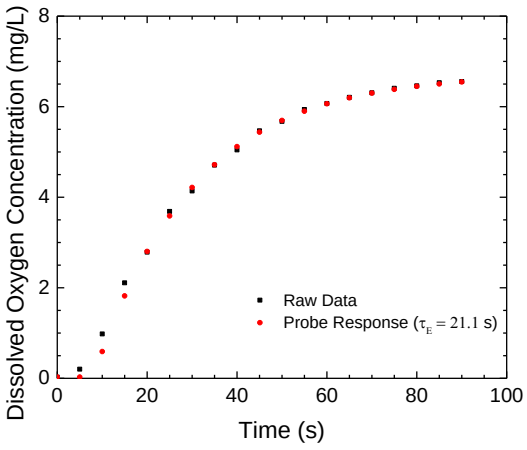

Figure 11: Probe time constant determination.

The time constant used in $k_L a$ determination was the average value of three replicate runs, and the associated error was 1.4%.